# The Mutual Interaction between External Rossby Waves and Thermal Forcing: The Subpolar Regions

ISIDORO ORLANSKI

*Atmospheric and Oceanic Sciences Program, Princeton University, Princeton, New Jersey*

SILVINA SOLMAN

*Centro de Investigaciones para el Mar y la Atmosfera, CONICET-UBA, Ciudad Universitaria, Buenos Aires, Argentina*

(Manuscript received 21 July 2009, in final form 22 January 2010)

ABSTRACT

The authors hypothesize a simple feedback mechanism between external Rossby waves and diabatic heating from convection. This mechanism could explain the large amplitude that external Rossby waves attain as they propagate to mid- and high latitudes. A series of experiments has been carried out with a core dynamic global spectral model. These simulations with the idealized atmospheric GCM and a simple parameterization of thermal forcing proportional to the low-level wave meridional velocity suggest that external Rossby waves can be enhanced by convection, which they themselves induce. It is shown that in the tropospheric upper levels the amplitude of the external waves can be twice as large with feedback as for a control simulation that does not allow feedback.

## 1. Introduction

The role and dynamics of large stationary and quasi-stationary atmospheric circulation has stimulated considerable discussion in the scientific community. Since the pioneering work of Charney and Eliassen (1949), Bolin (1950), and Smagorinsky (1953), there have been numerous studies on the effects of large-scale orography and thermal forcing on atmospheric flows. Charney and Eliassen emphasized the importance of orography on large-scale stationary disturbances over the midlatitude westerlies. However, Smagorinsky pointed out the importance of thermal forcing, suggesting that it is equally important in forming stationary waves. Since then, studies using models with different levels of complexity (e.g., Kasahara 1966; Egger 1976; Manabe and Terpstra 1974; Kasahara et al. 1973; and more recently, Held and Ting 1990) have demonstrated that orography and thermal forcing are both important for generating the stationary and quasi-stationary midlatitude waves in the atmosphere.

*Corresponding author address:* Isidoro Orlanski, Atmospheric and Oceanic Sciences Program, Princeton University, Princeton, NJ 08540.
E-mail: isidoro.orlanski@noaa.gov

DOI: 10.1175/2010JAS3267.1



A considerable number of studies have established that the extratropical stationary wave patterns in both hemispheres have an equivalent barotropic structure (e.g., Wallace and Blackmon 1983; Randel and Stanford 1983; Blackmon et al. 1979). Moreover, the interannual variability induced by the wavelike teleconnection of the El Niño–Southern Oscillation (ENSO) cycle has horizontal and vertical scales similar to those of stationary Rossby waves (Namias 1973; Wallace and Gutzler 1981; Horel and Wallace 1981; Dole 1983). The Southern Hemisphere (SH) polar waveguide has been frequently discussed in the literature as well. Studies of planetary waves in the Southern Hemisphere by Trenberth (1980) and teleconnections by Mo and White (1985) and Ambrizzi et al. (1995), among others, have described the presence of a pattern with a wavenumber equivalent to 3 or 4 near 55°S. These results were confirmed by Ambrizzi et al. (1995). Their data revealed wave propagation from the eastern South Pacific to the equatorial Atlantic in an arclike route, which is similar to the Pacific–South America (PSA) pattern discussed by Mo and Ghil (1987). Evidence of wave propagation from the east Pacific to the Indian Ocean has also been found (Gao and Stanford 1988).

Plumb (1985) pointed out that, if transient eddies are an important source of stationary wave activity, this

component of the stationary wave field could be generated by heat and vorticity flux divergences due to the transient eddies. Eddies might lead to stationary wave activity via direct interaction or latent heat release, which could result from longitudinal asymmetry of storm tracks. Tropical forcing could produce a ray of Rossby waves characterized by a quasi-stationary circulation that propagates around the globe in great circles (Grose and Hoskins 1979; Hoskins and Karoly 1981; Held 1983). However, it is known that the mean circulation and transient eddies could modify their propagation trajectories and, moreover, dissipate their energy. As discussed in Holopainen et al. (1982) and Lau (1979), the transient eddy time-mean heat fluxes dissipate and damp the stationary waves. Youngblut and Sasamori (1980) and Holopainen et al. estimated that transient eddy potential vorticity fluxes damp the stationary eddy potential enstrophy. Holopainen et al. estimated an *e*-folding time of 4–5 days averaged over the extratropical troposphere. It could be expected then that stationary eddies would be larger without the presence of the transient eddies. Held et al. (1986) suggested that the thermal boundary layer damping as well as the potential vorticity damping could, in fact, destabilize the external Rossby waves if the damping is larger at the lower boundary than in the free atmosphere.

Honda et al. (1999) explored the atmospheric response to anomalous sea ice numerically using an atmospheric general circulation model (AGCM) to examine the influence of anomalies in sea ice extent on the large-scale atmospheric circulation. For both heavy and light ice cases, the atmospheric response occurs not only in the region of the sea ice but far downstream in the form of a stationary wave train propagating along a great circle, extending the sea ice response from the polar regions to well into the middle latitudes.

In this paper we suggest a different mechanism for the enhancement of external waves. We demonstrate that external waves could be destabilized by diabatic heating and, in fact, that this diabatic heating may be due to convection organized by the external wave itself.

First, in section 2, we will show some examples of external wave patterns over the southeastern Pacific Ocean from an analysis of the National Centers for Environmental Prediction (NCEP)–National Center for Atmospheric Research (NCAR) reanalysis dataset and from solutions of the Geophysical Fluid Dynamics Laboratory (GFDL) AGCM. We then discuss our hypothesis describing why external Rossby waves that are remotely generated could interact with a thermal forcing, further enhancing the external wave. An abbreviated review of the spectral global atmospheric model and a description of a simple parameterization that was used to illustrate the mechanism of mutual interaction are presented in section 3. Model results that demonstrate the interaction process between a thermal forcing and the external wave are discussed in section 4. Finally, these results are summarized and discussed in section 5.

## 2. How quasi-stationary circulation is maintained

Quasi-stationary waves can be found all over the globe. However, since our discussion is related to the mutual interaction of diabatic heating and the external mode, we identify three regions of particular interest: (i) the *equatorial region* where the ITCZ is bounded by two high pressure systems, one in each hemisphere; (ii) the *storm-track regions* where a low pressure system is always found at the entrance of the storm track and a high pressure system at its end; and (iii) the *subpolar regions* where circulation around a high pressure system is found to advect moisture and heat to the polar ice caps. In this study, we focus on the subpolar regions because we found that thermal sources are more localized and therefore easier to describe.

A high pressure pattern over the southeastern Pacific Ocean is frequently observed associated with the warm phase of ENSO (Mo and Ghil 1987; Mo and Higgins 1998; Mo and Paegle 2001; Silvestri and Vera 2003). This high pressure system is associated with the PSA pattern, which appears to be located very close to the sea ice boundary of the SH. We will use this pattern as a prototype for exemplifying the mutual interaction between diabatic heating and the external wave pattern.

Mo and Paegle (2001) extensively studied the characteristics of the quasi-stationary circulation over the SH. They described two pervasive modes of atmospheric variability that influence circulation and rainfall over South America. They appear as leading empirical orthogonal functions (EOFs) of the 500-hPa height anomaly field or the 200-hPa streamfunction anomaly field and are found at intraseasonal to decadal time scales. Both patterns exhibit wave-3 hemispheric patterns in mid to high latitudes and a well-defined wave train with large amplitude in the PSA sector. Therefore, they are referred to as the PSA modes (PSA1 and PSA2). PSA1 is related to sea surface temperature anomalies (SSTAs) over the central and eastern Pacific at decadal scales in response to ENSO in the interannual band. PSA2 is associated with the quasi-biennial component of ENSO, with a period of 22–28 months. For the PSA2 mode, the strongest connections occur during austral spring. These two modes are also apparent in tropical intraseasonal oscillations for both summer and winter. Eastward propagation of enhanced convection from the Indian Ocean to the central Pacific is accompanied by a wave train that appears to

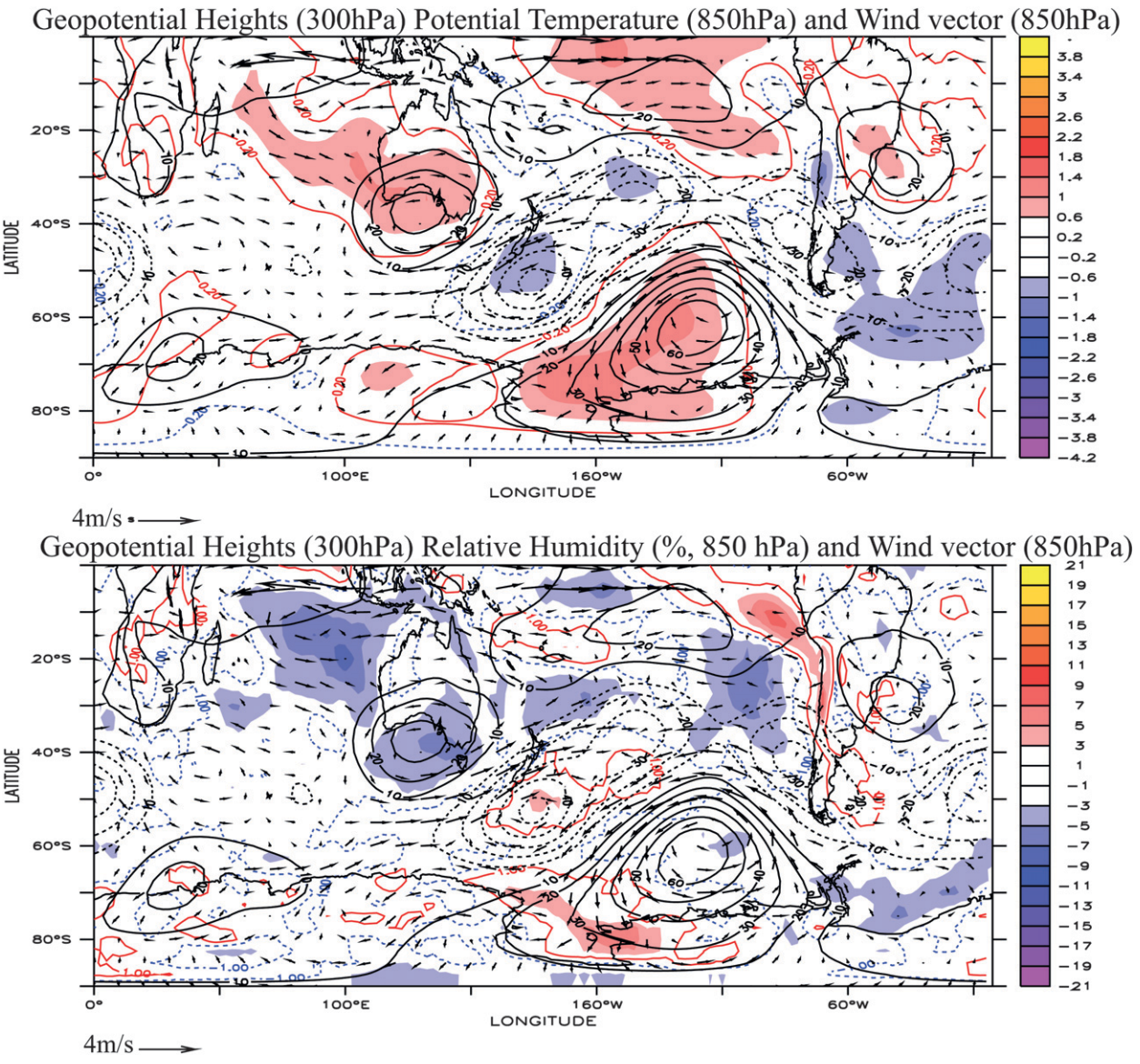


FIG. 1. Composite El Niño 3.4 index (above one standard deviation) of (a) 300-hPa geopotential heights, contour interval 10 m, and 850-hPa potential temperatures, shading interval 0.2 K; (b) 300-hPa heights and 850-hPa relative humidity, shading 2% contour. Both (a) and (b) show the 850-hPa wind anomalies. The reference arrow is 4 m $s^{-1}$.

originate in the convective regions. The positive PSA1 pattern is associated with enhanced convection over the Pacific from 150°E to the date line. The convection pattern associated with PSA2 due to the orthogonality constraint is in quadrature with that of PSA1. As was pointed out by Mo and Ghil (1987), this may be due to the atmospheric internal variability rather than the anomaly being forced only by equatorial SSTAs.

The composite patterns for different atmospheric variables for the warm phase of ENSO are shown in Fig. 1. Considerable high temperature and relative humidity are found on the southwestern side of the high anomaly where the poleward flow is dominant, over the periphery of Antarctica. This pattern is also consistent with the composite of the poleward surface winds owing to the strong equivalent barotropic structure of the height anomaly. Regression analysis also shows a reduction of sea ice in areas where high temperature anomalies are observed (Fig. 1a). It is believed that the latter is a consequence of warm advection (Venegas and Drinkwater 2001; Watanabe and Hasumi 2005; Deser et al. 2007).

Numerous studies have found a negative correlation between sea ice concentrations and ENSO variability (Simmonds and Jacka 1995; White and Peterson 1996;

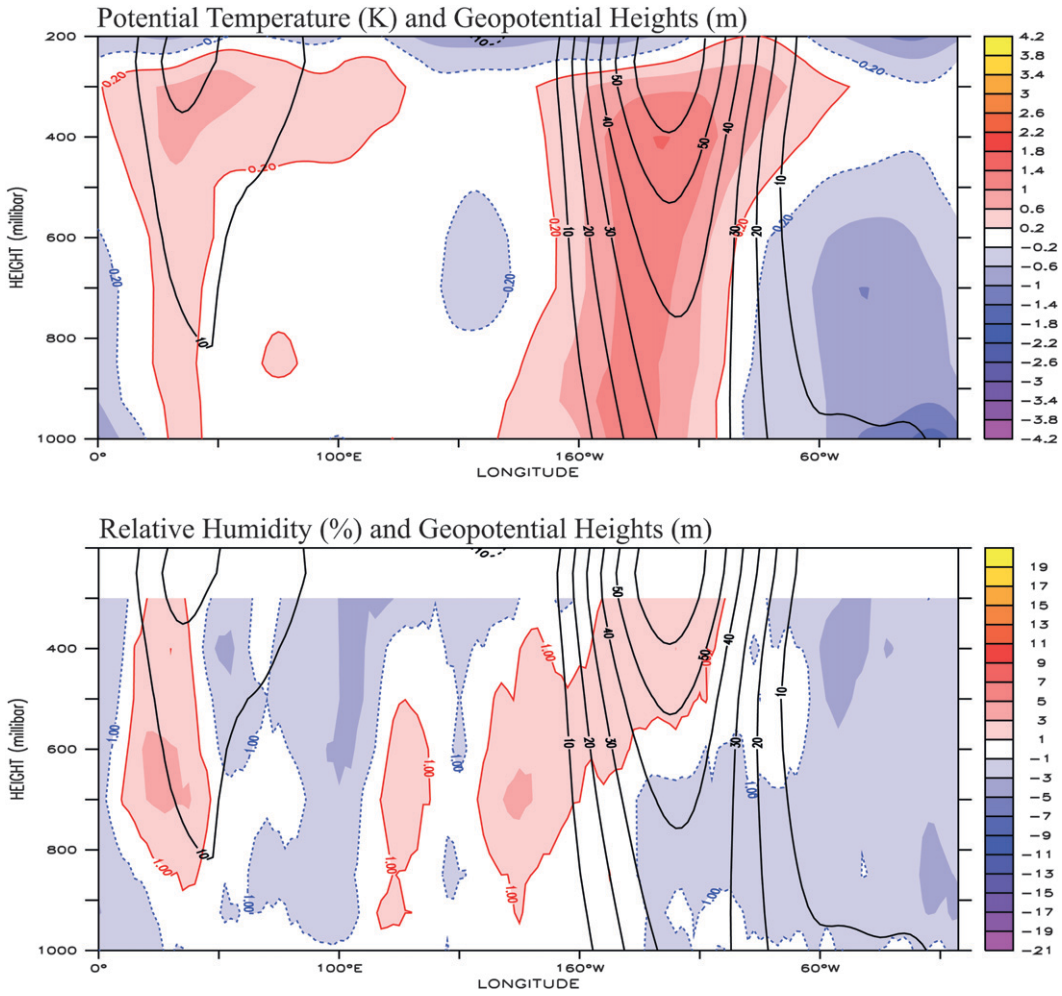


FIG. 2. Composite El Niño 3.4 index (above one standard deviation) for the cross sections at the maximum of the subpolar geopotential height, contour interval 10 m: (a) potential temperature anomaly, shading interval 0.2 K and (b) relative humidity, shading 2% contour.

Yuan 2004). Similar patterns of atmospheric circulation and sea ice have been found in various subpolar regions of both hemispheres (Venegas and Drinkwater 2001; Watanabe and Hasumi 2005; Deser et al. 2007).

We will focus on the increased precipitation and temperature due to the relatively warm, moist air blowing over a very cold surface rather than on the reduction of sea ice. In fact, regressions of the 300-hPa height with an index based on the average temperature over the Ross Sea show results similar to Fig. 1. These results imply that this geopotential height pattern occurs very frequently and that there are different mechanisms that generate a similar response.

The interpretation seems to be straightforward: the circulation associated with the high pressure system located over the subpolar regions produces advection of heat and moisture due to the poleward wind bringing warm, moist air into the cold Antarctic coast. Notably, the lower-level circulation in Fig. 1 is anticyclonic, in phase with the upper-level circulation (consistent with the equivalent barotropic structure shown in Fig. 2). The structures of the geopotential height and potential temperature shown (Fig. 2a) are very similar to those found in the correlation of SSTAs and geopotential heights over the storm tracks of the Northern Hemisphere (NH) (Kushner et al. 2002), which will be critical to our proposed mechanism.

To further illustrate the relative position of the geopotential height and temperature anomalies, we will show two solutions of the GFDL AM2 model described in Anderson et al. (2004). The control solution is based on prescribed conditions of the Second Atmospheric Model Intercomparison Project (AMIP II). This 30-yr simulation (Control) is contrasted with a similar run in where

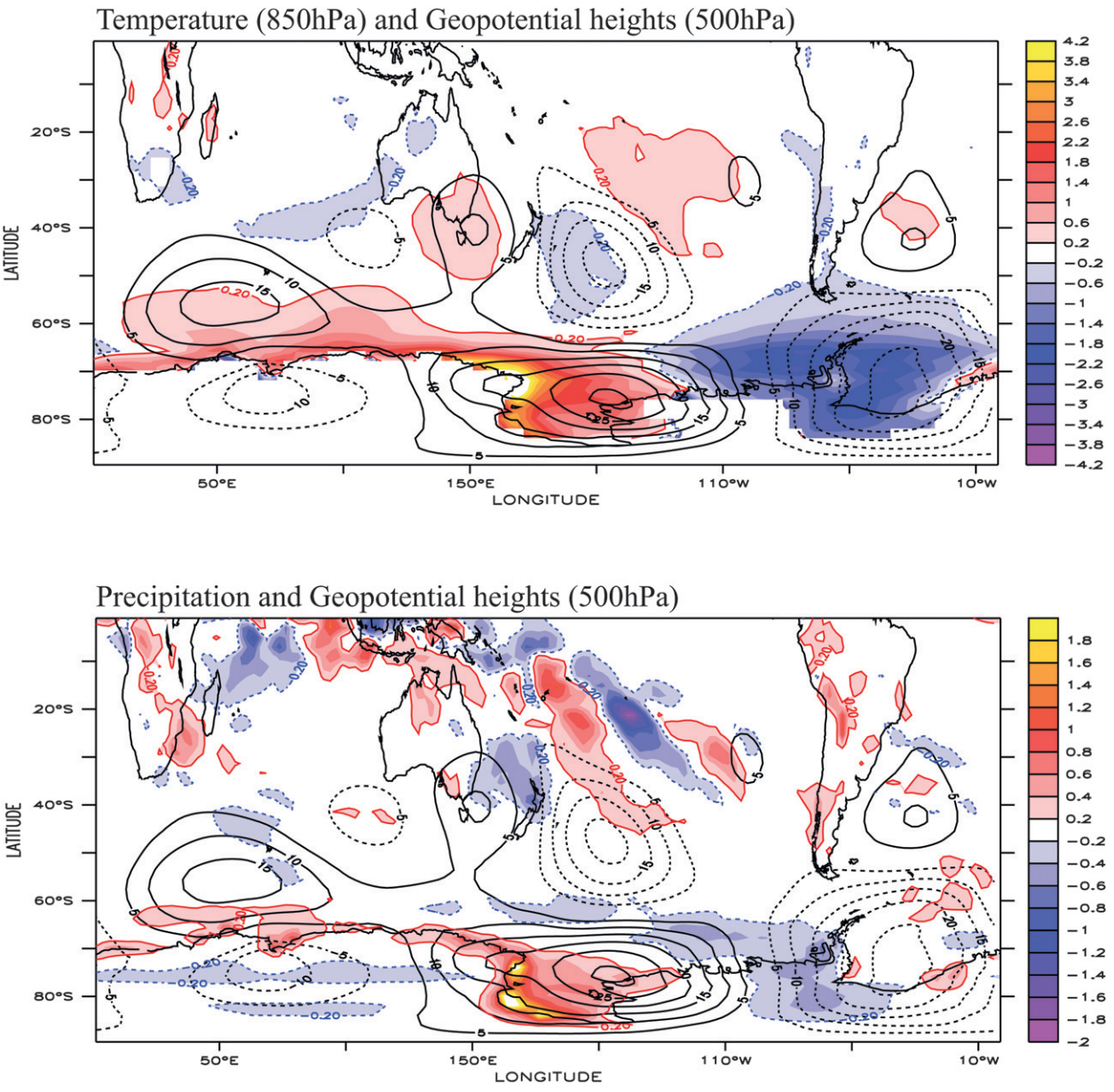


FIG. 3. Anomalies in the difference between the No–sea ice and control runs of the GFDL GCM averaged over a 30-yr window: (a) 500-hPa geopotential heights, contour interval 5 m, and air temperature, indicated by shading with interval 0.4 K, and (b) 500-hPa geopotential heights, contour interval 5 m and precipitation, indicated by shading, first contour 0.2 mm day$^{-1}$.

the sea ice has been set to zero (No sea ice). The simulation without sea ice is highly unrealistic because a climatological ocean surface temperature is used over the region without sea ice.

The differences in the geopotential height, surface temperature, and precipitation between the No–sea ice and Control runs for 30 seasons [September–November (SON)] are shown in Fig. 3. The differences are larger over the subpolar regions and the changes in the atmospheric circulation are clearly noticeable in the very high latitudes over the regions with different sea ice distributions. The height anomaly (at 500 hPa) and surface temperature are shown in Fig. 3a and precipitation in Fig. 3b. The relation of the height anomaly with the temperature and moisture fields is very similar to the patterns shown in Fig. 1. The geopotential heights have an equivalent barotropic structure similar to that shown in Fig. 2 and again, as in the ENSO response, the maximum temperature and precipitation values are found on the poleward wind region west of the height maximum.

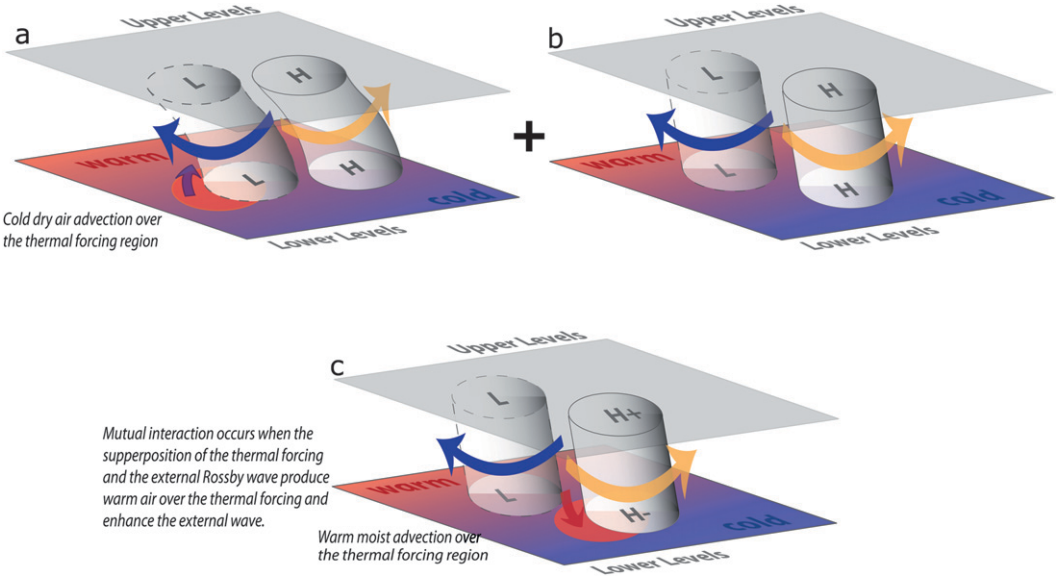


FIG. 4. The schematic diagram depicts two classic responses due to (a) thermal forcing and (b) remote forcing. (c) The interaction between the external wave and local thermal forcing. In (a) is shown a baroclinic response to the thermal forcing (red surface ellipsoid); in this case, the low-level wind (dark blue arrow) advects cold dry air over the thermal forcing region. In (b) is shown a system of highs and lows remotely generated by a tropical source. In (c) the superposition of both mechanisms—remote forcing and thermal forcing—shows that the lower-level wind (red arrow) could advect warm moist air into the thermal forcing region (red ellipsoid) that reinforces the heat source and enhances the upper-level external wave, indicated by H+; at lower levels, since the thermal forcing tends to produce a low pressure center, the external wave high show a diminished heating, H−.

The vertical distribution of the diabatic heating is important in discussing the thermal forcing on external Rossby waves. The column diabatic heating can be estimated from precipitation, but it is also important to know the vertical distribution of the forcing. These simulations allow us to explore the vertical distribution of diabatic heating, a field that cannot be produced from reanalysis data. From the GCM results we estimated the diabatic heating (not shown) extending from the surface to above 800 hPa in the area where the maximum precipitation occurs (Fig. 3b).

The steep Antarctic orography may play a role in the difference response between the No–sea ice and Control simulations, shown in Fig. 3, even if the two simulations have the same topography. The external waves are sensitive to the mean zonal flow, and the response could have been influenced to some degree by the topography under these conditions. However, there is a clear relationship between the temperature and humidity fields, the downstream geopotential height anomaly from reanalysis composites (Figs. 1 and 2), and the GCM simulations with and without sea ice (Fig. 3). Moreover, similar relationships between thermal sources and height anomaly fields have been described in the literature for SSTAs along storm tracks (a good summary can be found in the review article by Kushner et al. 2002).

Let us then describe a possible working hypothesis of how a mutual interaction between the external Rossby waves and a confined region of convection might occur. The schematic of Fig. 4 describes the elements needed for the interactive mechanism to work. As described in Hoskins and Karoly (1981), at lower tropospheric levels the thermodynamic energy equation determines the pattern of the response: the heating is balanced by either zonal or meridional temperature advection, depending on the depth of the heating. For deep heating, meridional advection dominates, requiring a downstream shift in the surface low. For shallow heating, zonal advection is also important, requiring a baroclinic warm core structure, shifted downstream from the heat source. Basically this process is portrayed in the schematic of Fig. 4a. The surface low is downstream of the heat source and tilted to the west aloft. Neither the response shown in Figs. 1–3 nor the patterns described in Kushner et al. (2002) for the response to SSTAs displays such a baroclinic response. Instead, the response has an equivalent barotropic structure and there is an anticyclone slightly downstream of the heat source.

It is clear that, if the equatorward circulation over the thermal forcing has a structure similar to that shown in Fig. 4a, the response could not produce a reinforcement of the thermal forcing because the wave would bring

cold dry air over the thermal source region. The only possibility for the external wave response to produce an enhancement of the thermal source is if the circulation over the source region is poleward. It is well known that the response to transient eddy vorticity fluxes can reverse the linear, near-surface response to shallow heating, replacing a baroclinic low pressure anomaly downstream with an equivalent barotropic high (Kushner et al. 2002). At upper levels, the vorticity equation determines the balance, and the potential vorticity sink can be balanced either by zonal advection, implying a low west of the heating and a high downwind, or by meridional advection across the mean potential vorticity gradient, implying a downstream low.

As was shown by Kushner et al. (2002), for a horizontal scale typical of a SST anomaly, zonal advection dominates, producing a downstream high (Hoskins and Karoly 1981; Hendon and Hartmann 1982; Held 1983). A similar effect could be obtained if one considers an external Rossby wave that has been remotely generated, as shown in Fig. 4b. The linear superposition of both the effects of the thermal source and the barotropic response of the remotely generated wave could change the circulation in the near-surface levels to make it anticyclonic with poleward flow over the thermal region. The advected moist, warm air would supply fuel that could reinforce the convection in the region and thereby enhance the external wave response, as suggested in Fig. 4c. This is our hypothesis for the process leading to mutual interaction between a remotely generated external wave and the convection organized by the wave.

We will perform simulations with a spectral GCM under much idealized conditions and minimal physics to evaluate the possibility that, indeed, there is a mutual interaction between the quasi-stationary circulation and the thermal forcing.

## 3. Model details and thermal forcing

The spectral model as described in Held and Suarez (1994)[1] was used to compare benchmark simulations in order to evaluate different atmospheric general circulation models independently of physical parameterizations. The model is a standard hydrostatic, $\sigma$-coordinate, semi-implicit, spectral transform model, in vorticity–divergence prognostic equations. The transform grid is chosen to ensure alias-free computation of quadratic products. The vertical differencing uses the simplest centered differences, and the hydrostatic equation is integrated analytically assuming that temperature is constant within each layer. There are 20 vertical levels, equally spaced in sigma, with the top of the model formally set to a zero pressure. A leapfrog scheme is used for a time-stepping time filter to control the computational mode. The horizontal mixing of vorticity, divergence, and temperature takes the form of a Laplacian raised to the fourth power, with the strength set so that the *e*-folding time for the smallest wave in the system is always 0.1 days. The truncation is triangular. All integrations shown are for T63 resolution.

### a. Model equations

The Held–Suarez (1994) model uses the standard primitive equations:

$$\frac{D}{dt}\mathbf{v} = [2\sin(\varphi) + u\tan(\varphi)/a]\mathbf{k} \times \mathbf{v} - \frac{1}{\rho}\nabla p + k_v(\sigma)\mathbf{v};$$
$$\frac{D}{Dt}T = \frac{\kappa T\omega}{p} + k_T(\varphi, \sigma)[T - T_{\text{eq}}(\varphi, \sigma)];$$
$$\frac{D}{Dt} = \frac{u}{a\cos(\varphi)}\frac{\partial}{\partial\lambda} + \frac{v}{a}\frac{\partial}{\partial\varphi} + \omega\frac{\partial}{\partial\sigma}; \tag{3.1a}$$

where $\mathbf{v} = (u, v)$ is the wind vector with $u$ and $v$ the zonal and meridional components, $\omega$ is the traditional notation for $Dp/Dt$, $\kappa = R/c_p$ in which $R$ is the ideal gas constant and $c_p$ is the heat capacity at constant pressure, and $T$ is the air temperature and $T_{\text{eq}}$ the equilibrium temperature defined below. In the spectral model it is quite convenient to use the traditional Phillips sigma-coordinate $\sigma = p/p_o$, previously defined as a terrain-following coordinate.

The hydrostatic approximation is

$$\frac{\partial\Phi}{\partial\ln p} = -RT, \tag{3.1b}$$

and the integration of the conservation of mass in pressure coordinates with the use of the hydrostatic approximation provides the pressure condition at the surface:

$$\frac{\partial p_s}{\partial t} = -\nabla\cdot\int_o^{p_s}\mathbf{v}dp. \tag{3.1c}$$

The system of equations (3.1a)–(3.1c) constitutes the primitive equations with the standard approximation and provides the full system of the spectral model.

The control conditions are those described for the climate benchmark (Held and Suarez 1994):

[1] The code for this model is available upon request (e-mail Isaac.Held@noaa.gov).

$$T_{\rm eq} = \max\left\{200\,{\rm K}, \left[315\,{\rm K} - (\Delta T)_y \sin^2\varphi - (\Delta\theta)_z \log\left(\frac{P}{P_0}\right)\cos^2\varphi\right]\left(\frac{P}{P_0}\right)^{\kappa}\right\};$$

$$k_T = k_a + (k_s - k_a)\cos^4\varphi \max\left[0, \frac{\sigma - \sigma_b}{1 - \sigma_b}\right];$$

$$k_v = k_f \max\left[0, \frac{\sigma - \sigma_b}{1 - \sigma_b}\right];$$

$$\sigma_b = 0.7, \quad (\Delta T)_y = 60\,{\rm K}, \quad (\Delta\theta)_z = 10\,{\rm K},$$

$$k_f = 2,\ 1,\ 0.5\ {\rm day}^{-1}, \quad k_a = \frac{1}{40}{\rm day}^{-1}, \quad k_s = \frac{1}{4}{\rm day}^{-1}.$$

The temperature is relaxed to a prescribed "radiative equilibrium," $T_{\rm eq}$. Here $T_{\rm eq}$, the Raleigh friction coefficient $k_f$, and the Newtonian cooling coefficient for the interior atmosphere $k_a$ and in the boundary layer $k_s$ are taken from Held and Suarez (1994).

### b. The experimental setting

#### 1) THE FORCING FOR THE CONTROL RUN

Since the model represents only a dry atmosphere (only the dynamical core), to simulate the effect of the diabatic heating produced by the SSTs and waves we should include two sources of heat: one equatorial and one interactive over the subpolar region of the SH. The equatorial one will generate a train of external Rossby waves similar to the equatorial convection produced by the warm phase of the ENSO SSTAs. The subpolar one portrays the advection of moisture by the remotely generated external Rossby wave train and will be proportional to the wave low-level meridional velocity. The thermodynamical equation is given by

$$\frac{\partial}{\partial t}T = \cdots k_T(\varphi, \sigma)[T - T_{\rm eq}(\varphi, \sigma)] + \frac{\partial}{\partial t}F_{\rm polar} + \frac{\partial}{\partial t}F_{\rm equatorial}. \qquad (3.2)$$

The equatorial forcing has the form

$$\frac{\partial}{\partial t}F_{\rm equatorial} = (\Delta\theta)_t \exp\left[-\left(\frac{x - x_0}{x_{\rm wid}}\right)^2\right]\exp\left[-\left(\frac{y - y_0}{y_{\rm wid}}\right)^2\right] \times 0.5\left[1. + \tanh\left(\frac{P - \delta P_0}{P_{\rm th}}\right)\right], \qquad (3.3)$$

where $dF_{\rm equatorial}/dt$ represents the deep diabatic forcing for the equatorial region simulating the SST anomaly of the ENSO warm phase. The amplitude is $\Delta\theta_t$ (assumed to be around 1 K day$^{-1}$), $x_{\rm o}$ and $y_{\rm o}$ ($x_0 = 160$°E longitude and $y_0 = 0$° latitude) are the center of the forcing, with a decay in the zonal direction $x_{\rm wid} = 30$° and latitudinal direction of $y_{\rm wid} = 10$°. The vertical distribution is maximum at the ground, with a decay thickness of $P_{\rm th} = 50$ hPa centered at $\delta P_0 = 500$ hPa.

The polar forcing is similar to that of Eq. (3.3) but zonally symmetric:

$$\frac{\partial F_{\rm polar}}{\partial t} = K(y, p).$$

The expression of $K(y, p)$ is similar in the meridional and vertical extension to that previously used in Eq. (3.3). The control solution then will be run, forced with the equatorial forcing [Eq. (3.3)] and a mean zonal thermal forcing function given as

$$\frac{\partial}{\partial t}F_{\rm polar} = \left\langle\frac{\partial}{\partial t}F\right\rangle = (\Delta\theta)_t \exp\left[-\left(\frac{y - y_0}{y_{\rm wid}}\right)^2\right] \times 0.5\left[1.0 + \tanh\left(\frac{P - \delta P_0}{P_{\rm th}}\right)\right]. \qquad (3.4)$$

Note that a forcing of that form [Eq. (3.4)] with zonal-mean average equal to $K(y, p)$ should affect the zonal flow because it will affect the zonal-mean temperature field. The reason to choose such an expression will soon be apparent when we discuss the thermal forcing for the interactive case. Since the external Rossby waves are so sensitive to the zonal flow, it will be difficult to compare an interactive simulation with a control solution if the control solution lacked thermal forcing.

#### 2) THE FORCING OF THE INTERACTIVE RUN

The polar forcing is an idealization of the meridional advection of moisture:

$$\frac{\partial}{\partial t}F_{\rm polar} = K(y, p)^* G(V_{\rm wave}), \qquad (3.5)$$

where $K(y, p)$ is the zonally symmetric component of the heating function [Eq. (3.4)] and $G(V_{\rm wave})$ is the wave component meridional velocity that will affect the amplitude of the thermal forcing, with the zonal average of $\langle G(V_{\rm wave})\rangle = 1$. This condition assures equality between the zonal mean forcing for all cases.

A simple approach could have been to force the interactive simulations without a zonal mean forcing. This approach would have given positive and negative forcing (warming and cooling): the warming could be justified because of the cumulative effects of latent heating produced by moist convection. However, there is not justification for the presence of cooling. In the present approach, the control simulation will have a zonal heating in the subpolar latitudes that modifies the circulation in those regions. However, the zonal mean effect is the same for the perturbed interactive simulation. We use an expression for the interaction $G(V_{\text{wave}})$ such that the zonal average will be equal to unity, as previously mentioned:

$$\frac{\partial}{\partial t} F_{\text{polar}} = (\Delta\theta)_t \exp\left[-\left(\frac{y - y_0}{y_{\text{wid}}}\right)^2\right] 0.5\left[1. + \tanh\left(\frac{P - \delta P_0}{P_{\text{th}}}\right)\right] G(V_{\text{wave}}),$$
$$G(V_{\text{wave}}) = [1.0 - V'(t, x, y, p_1)/V_0], \quad \langle G(V_{\text{wave}})\rangle = 1,$$
$$V' = V - \langle V\rangle, \tag{3.6}$$

where $V'$ is the deviation from the zonal mean meridional velocity, at a specific level $P_1 = 750$ hPa and $V_0$ is a parameter that controls the feedback of the forcing, such that $G(V_{\text{wave}})$ is mostly positive. In this way, no unrealistic cooling will occur and the Control simulation and the interactive one will have the same zonal thermal forcing to assure that the zonal mean circulations are not very different from each other. The amplitude is $\Delta\theta_t$ (assumed to be around 2 K day$^{-1}$) and $y_o$ (65°S) is the center of the forcing, with a decay in the latitudinal direction of $y_{\text{wid}} = 10°$. The vertical distribution is maximum at the ground, with a decay with a thickness $P_{\text{th}} = 50$ hPa centered at $\delta P_0 = 800$ hPa.

It should be stressed that all solutions, control and interactive, use the same equatorial forcing for the generation of the external Rossby wave train. In this configuration, the perturbed waves will propagate over the globe with a zonal flow very similar to the Control solution. The parameterized heating [Eq. (3.6)] has some similarity to the well-known formulation of conditional instability of the second kind (CISK) (Charney and Eliasen 1964). CISK was designed to simulate the effect of waves in generating convection for the tropical atmosphere. The low-level convergence of the wave field produced convection and release of latent heat that, in turn, enhances convergence and further increases convection. The atmospheric environment that favors CISK is found over warm tropical oceans where there is an abundant supply of moisture and convergence is strong. In later development of CISK, only the ascending vertical velocity was used at the top of the boundary layer. This was done so as to eliminate the unrealistic cooling generated from the descending vertical velocity (Lindzen 1974 and others). In a similar fashion, we use Eq. (3.6) to prevent such unrealistic cooling. In the extratropics, the meridional advection of heat and moisture become more important, especially when the air blows over a cold surface characteristic of the subpolar regions.

We will discuss three solutions over the 2000-day runs: the *Control*, the *Interactive*, and the *Constant* simulations. The Control experiment was run for 1000 days with the subpolar zonal forcing described in Eq. (3.5). The 1000-day run was used as initial conditions to run for 2000 additional days for each of the three experiments. In the Control case, the simulation is continued with no changes in the zonal subpolar thermal forcing. The Interactive case has the same initial conditions as in Control but with a time-dependent thermal forcing, defined in Eq. (3.6). Finally, the Constant solution was obtained by running the model with the long-time-averaged forcing of Eq. (3.6) produced by the Interactive solution and held constant for the time of integration. It should be stressed then that the Interactive and Constant simulations have the same time averaged forcing; the only difference is due to transience in the Interactive forcing.

## 4. Results of the three simulations

### *a. The Control simulation*

The Control simulation is unrealistic because it has a zonal heat source over the subpolar regions. The only reason to use such a Control solution, as previously discussed, is to have a basis by which to evaluate the intensity of the feedback when the external wave is allowed to interact with the thermal source. In that context, one should consider the Control solution as an idealized state if the sea ice has been completely removed and warmer oceans are exposed to the cold subpolar air.

The top graph of Fig. 5 shows the cross section of the mean zonal velocity and potential temperature field averaged for the 2000-day period for the Control simulation. The middle graph of Fig. 5 shows the zonal mean

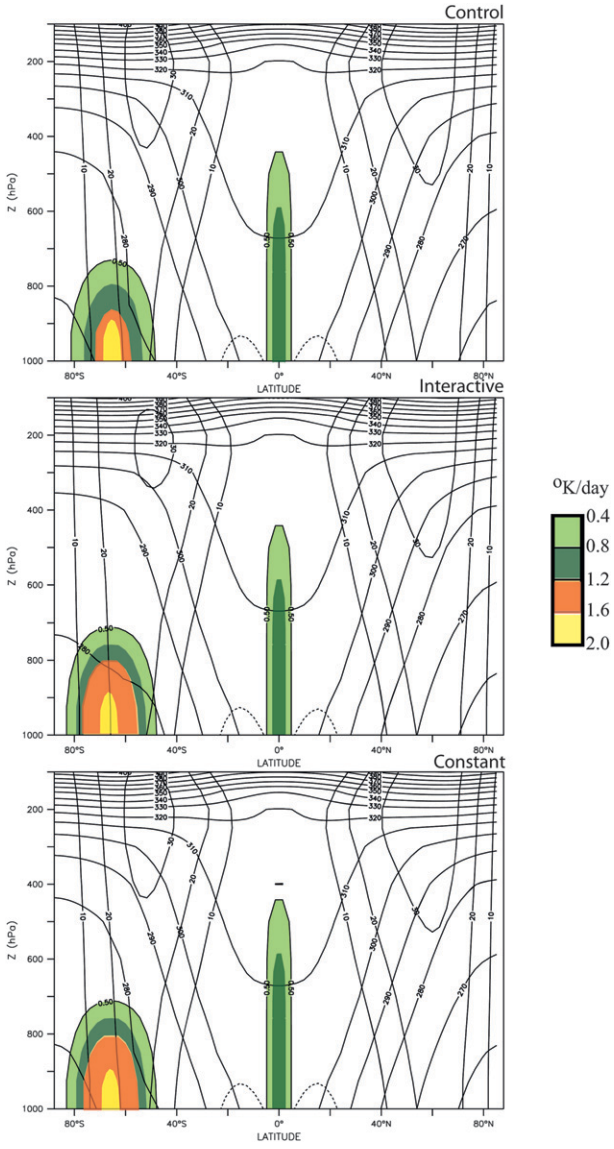


FIG. 5. The zonal mean conditions for the (top) Control, (middle) Interactive, and (bottom) Constant runs: the zonal wind (contour 10 m $s^{-1}$), potential temperature (contour 10 K), and subpolar thermal forcing (color shading). The equatorial thermal forcing is shown as a cross section at the center of the forcing $x = 160°$E. The thermal forcing contour shown is 0.4 K $day^{-1}$, the equatorial maximum is 1 K $day^{-1}$, and the subpolar is 2 K $day^{-1}$. The horizontal parameters for the subpolar forcing are $y = 65°$S with $y_{wid} = 10°$, with a decay height at 0.8 Pa. The equatorial forcing is located at $x = 160°$E with $x_{wid} = 30°$ and $y_{wid} = 5°$ and decay height at 0.4 Pa (see text for definitions).

flow for the Interactive case; finally, in the bottom graph in Fig. 5 the zonal flow for the Constant case is shown. Note the similarity of the zonal mean flow between the Control and Constant solutions; the small difference noticed with the Interactive solution is due to eddy transients. The steady response of the Control simulation can be seen in the top graph of Fig. 6, which shows the asymmetric zonal part of the 300-hPa geopotential height averaged for the period of 2000 days. The color-shaded regions indicate the equatorial [Eq. (3.3)] and subpolar thermal forcing [Eqs. (3.5)–(3.6). Notice that the external wave arch produced by the propagation emanating from the equatorial source region and the position of the upper-level geopotential height in the subpolar region somewhat resemble those shown in Fig. 1.

### b. *The Interactive and Constant thermal forcing simulations*

We have run a number of simulations using the forcing shown in Eq. (3.6) with different forcing intensities $V_0 = \{10, 5, 3, 2\}$. The Interactive and Constant simulations have the same starting data as in Control. They were run for 2000 days in time sections of 250 days. The bottom graph in Fig. 6 shows the 2000-day time-averaged solution for the Interactive case (with $V_0 = 2$). The thermal forcing (shaded region) is no longer zonal, as it was in the Control run, which shows the effect of the polar advection of heat due to the stationary response. The amplitude of the geopotential height anomaly at upper levels is substantially larger than for the Control run, especially over the SH subpolar region. The Northern Hemisphere waves are essentially unaffected by the thermal interaction with the SH wave. The solution with Constant heating is shown in the middle graph of Fig. 6. The general characteristics of the three solutions are very similar, at least for the upper-level response. The stationary component of the thermal forcing is, as previously discussed, the same as for the Interactive and Constant solutions. As expected, the largest difference is over the southern forcing area in which the difference between the Interactive and Control solutions displays a more intense system (Fig. 6). The bottom graph of Fig. 7 shows the anomalous height pattern and thermal forcing for the Interactive − Control cases. The anomalous heating of the Interactive − Control shows a positive anomaly on the west of the high anomaly and a negative anomaly on its eastern side, as expected from the poleward circulation over the west and equatorward circulation over the east.

In contrast, the Constant − Control cases show the 300-hPa height anomaly 180° out of phase with the thermal forcing (top graph of Fig. 7). It should be noted that the thermal forcing anomaly has positive and negative regions only because the zonal Control thermal forcing is subtracted.

The cross section of the difference between the Constant and Interactive simulations and the Control are shown in Figs. 8 and 9. The height anomalies over the latitudes of the maximum polar thermal forcing are shown

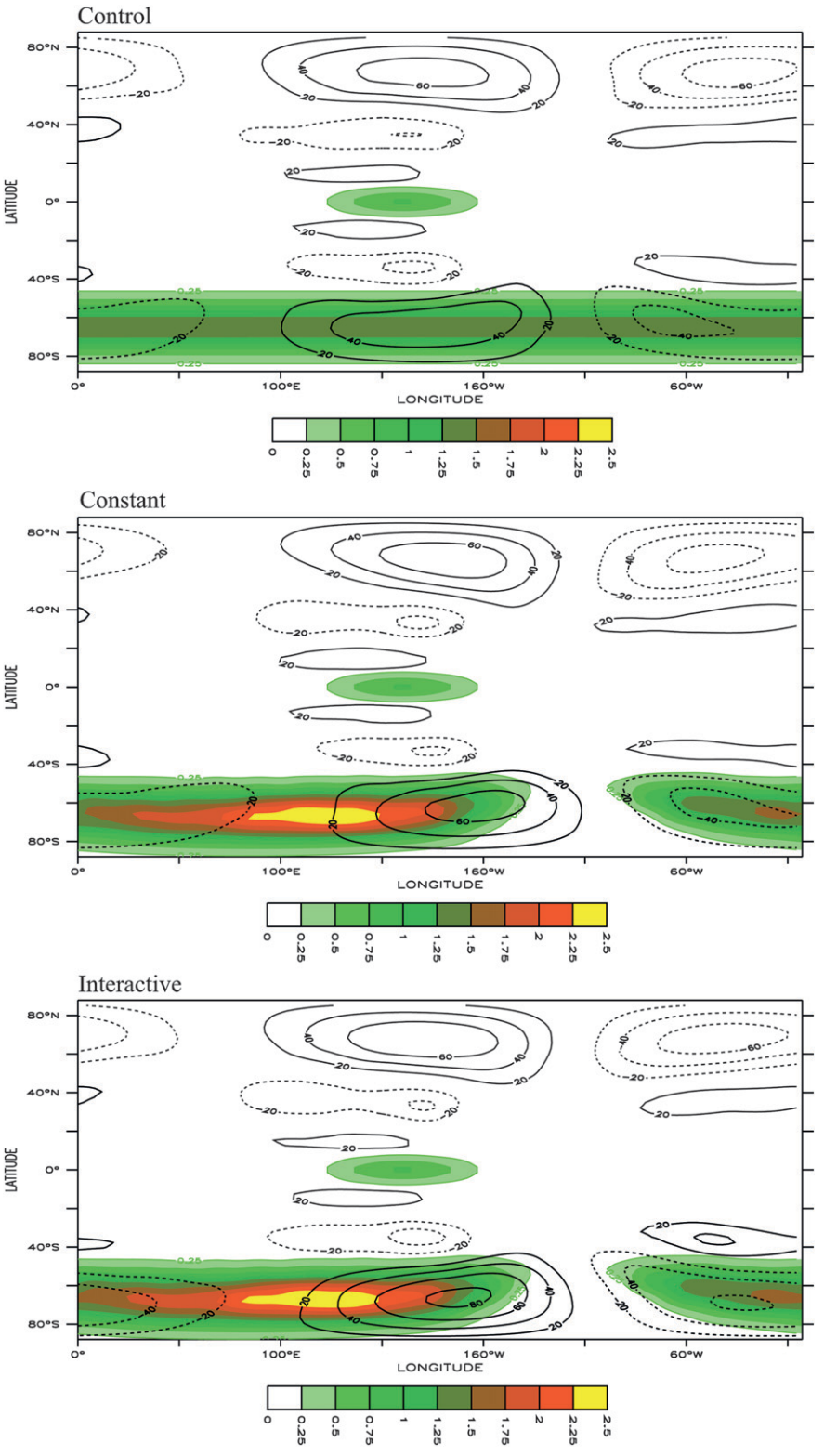


FIG. 6. The 2000-day averaged height anomalies at 300 hPa for the Control, Constant, and Interactive simulations in response to the thermal forcing (shown in color shading at $z$ = 850 hPa): (a) Control simulation with noninteractive heating, the subpolar forcing; (b) the Constant solution with time-constant thermal forcing (time mean averaged Interactive forcing), and (c) the Interactive simulation with the resulting forcing heating distribution due to the interaction, strength of the interaction $V_0 = 2$ (see text).

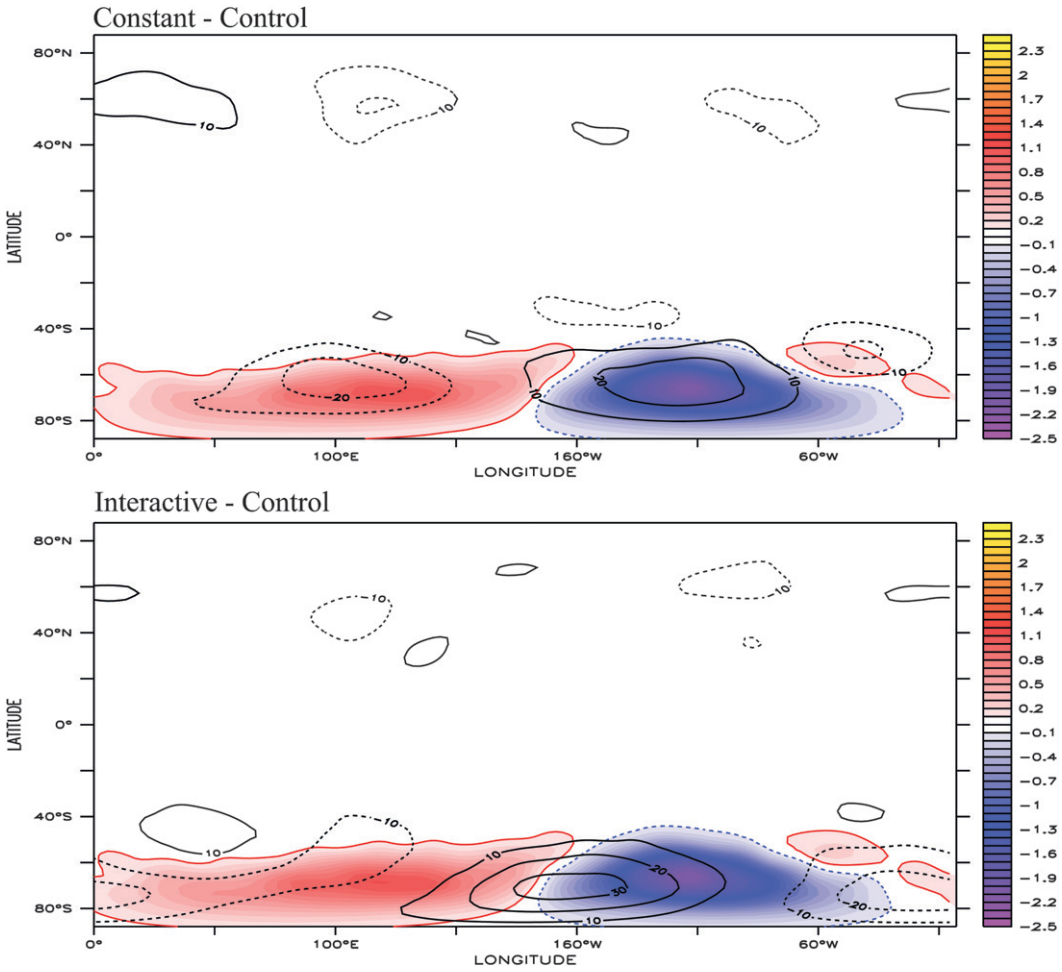


FIG. 7. Difference between the Constant and Interactive solutions with respect to the Control simulation are shown. Geopotential height anomaly (contour 10 m) and thermal forcing anomaly for the (a) Constant − Control and (b) Interactive − Control cases. Note that the forcing anomaly has positive (red) and negative (blue) regions because the sensitive runs were subtracted the zonal forcing of the Control case.

in Fig. 8. The Constant − Control anomalies display a tilted structure similar to the response of thermal forcing simulations reported in the literature (Hoskins and Karoly 1981; Hendon and Hartmann 1982; Held 1983), whereas the difference between the Interactive and Control seems more barotropic and in quadrature with the thermal source at all levels. This result is as expected since the parameterization of the thermal forcing by design is proportional to the meridional wind component of the stationary wave. The stationary response of the potential temperature anomaly shows a complementary view of the similarities and differences between the two anomalies as shown in Fig. 9. Whereas the Constant − Control simulation displays a low pressure center with a warm core anomaly, the Interactive − Control shows a high pressure center with a warm core anomaly. Note that the phase difference between the potential temperature and geopotential height of the Interactive − Control seems quite similar to that of the ENSO regression shown in Fig. 2. It should be stressed that the only difference between Interactive and Constant heating because of the time dependence in the Interactive simulation.

### c. *The linear response*

In spite of the large differences between the Interactive and Constant anomaly solutions shown in Figs. 7–9, the full responses shown in Fig. 6 are rather similar. This implies that the large barotropic structure of the total response is due to tropical forcing. It will be shown that the mechanisms that operate in these cases are similar and could be derived from linear balance concepts. As discussed in Hoskins and Karoly (1981) and Held (1983), the linear response to local thermal forcing is determined by the heat balance equation. Let us then

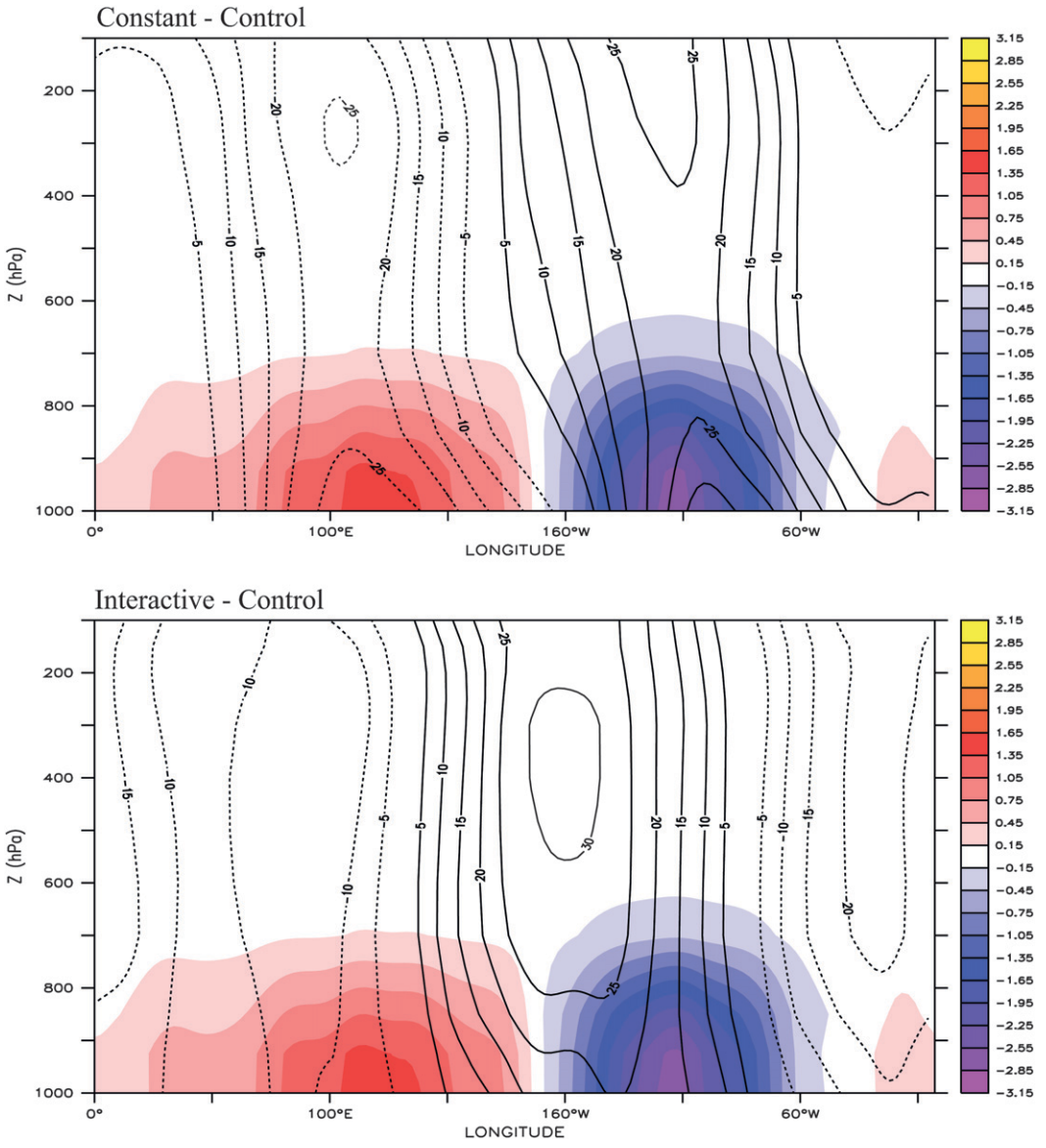


FIG. 8. Cross section at the center of the thermal forcing (65°S) of the geopotential height anomaly and thermal forcing for the (a) Constant − Control and (b) Interactive − Control cases, geopotential height contour 5 m. The thermal forcing is 0.3 K day$^{-1}$.

write the time-averaged heat balance equation to complete the discussion of the external wave response:

$$\overline{u\theta_x} + \overline{v\theta_y} + \overline{\omega\theta_p} = \overline{Q} - [\overline{(u'\vartheta)_x} + \overline{(v'\vartheta)_y}]_{\text{trans-eddies}} + \text{diss}, \qquad (4.1)$$

where $u$ and $v$ are wind components; $\theta$ is the potential temperature of the stationary component; $u'$, $v'$, and $\vartheta$ are the wind and the potential temperature of the transient eddies; $Q$ is the total diabatic forcing; and diss is the thermal dissipation. The overbar indicates the time average and the second term on the right is the divergence of the transient heat flux. We split the left-hand side into the predominant linear terms and the divergence of the stationary heat flux for the asymmetric part of the response and thermal forcing:

$$\overline{\overline{U}^z\theta_x} + v\overline{\frac{d}{dy}\overline{\Theta}^z} + \overline{(u\theta_x + v\theta_y)_{\text{SE}}} + \omega\overline{\frac{d}{dp}\overline{\Theta}^z} = \overline{Q}_{\text{thermal}} + \overline{Q}_{\text{vort}} - [\overline{(u'\vartheta)_x} + \overline{(v'\vartheta)_y}]_{\text{te}} + \text{diff}. \qquad (4.2)$$

The $z$ overbar indicates the zonal averaged quantities. As discussed in Hoskins and Karoly (1981) and Held (1983), the diabatic heating alone should be balanced by

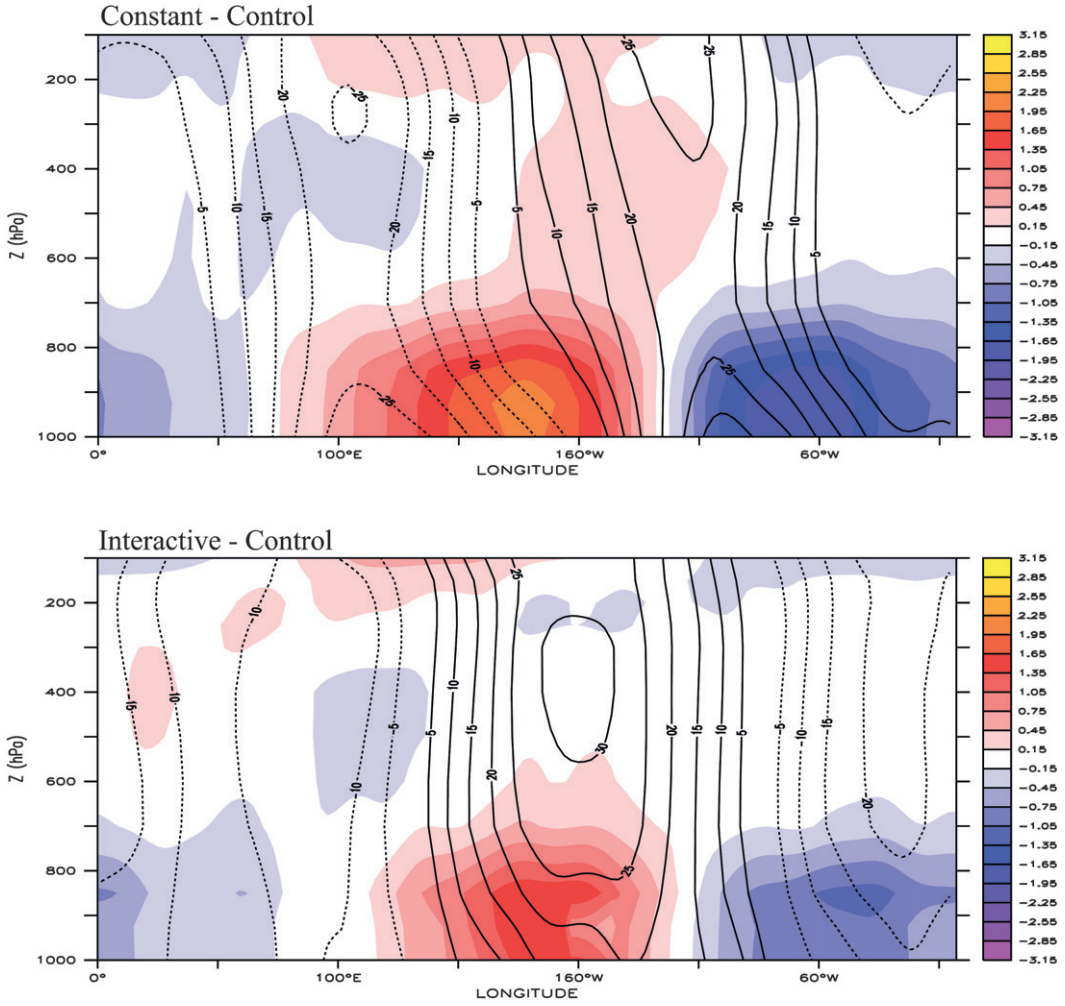


FIG. 9. As in Fig. 8 but for potential temperature (contour is 0.3 K day$^{-1}$).

the horizontal advection of heat at middle and high latitudes. Following Held (1983), we can write the quasi-geostrophic linear system for the lower levels with $Z = H \ln(P_*/P)$, only retaining the linear terms of Eq. (4.2). Note that the transient eddies terms are not negligibly small, and their importance will be discussed later in this section. Following Held (1983), the heat balance is maintained by the linear horizontal advection:

$$\begin{aligned} \overline{U}\theta_x + v\overline{\Theta}_y &= \kappa Q; \\ -f\overline{U}_z &= -\frac{g}{\Theta_0}\overline{\Theta}_y; \\ -fv_z &= \frac{g}{\Theta_0}\theta_x. \end{aligned} \tag{4.3}$$

The first equation in Eq. (4.3) is the linear heat advection [first two terms of the horizontal heat advection of Eq. (4.2)] that balances the thermal forcing; $Q$, $U$, and $v$ are zonal mean and meridional wave velocities, respectively, and $\theta$ is the potential temperature response. Note that the thermal wind relations in the last two equations are assumed for the SH ($f < 0$). Replacing the thermal wind balance in the heat equation we get

$$\begin{aligned} -\overline{U}v_z + v\overline{U}_z &= +\frac{g}{|f_0|}\kappa\frac{Q}{\Theta_0} = R; \\ -\overline{U}^2(v/\overline{U})_z &= R; \\ v_{\text{part}} &= +\overline{U}\int_z^\infty R/\overline{U}^2\, dz. \end{aligned} \tag{4.4}$$

The left side of the first equation in Eq. (4.4) is obtained by using the thermal wind relation. Note that these terms could be reduced to $-\overline{U}v_z + v\overline{U}_z = -\overline{U}^2(v/U)_z$, as shown on the left of the second equation. Finally, the meridional wind component of the particular solution to the thermal forcing can be obtained by integrating the

expression containing the diabatic forcing and the zonal mean wind component assuming that $v_{\text{part}}(\infty) = 0$. For a thermal forcing that has the same sign along the column and is positive, it is easy to deduce that the meridional wind component for the forced response should be equatorward (positive for the SH; it will be opposite for the NH). As previously mentioned, this circulation by itself will advect colder dry air over the thermal forcing region and consequently would not support the idea that an external wave could organize moisture and subsequent convection in the part of the wave that would be optimal for a positive feedback.

In a similar fashion, we could estimate the linear equivalent barotropic solution (without the thermal forcing; $R = 0$) or the homogeneous solution derived from the remote forcing (tropical heating):

$$v_{\text{baro}}(x, y, z) = v(z = 100\,\text{hPa}) \times \exp\left[-\int_z^{100}\left(\frac{\overline{g\Theta_y}}{|f_0|\Theta_0}\right)\Big/\overline{U}(z, y)\,dz\right]. \tag{4.5}$$

To satisfy the boundary condition the particular solution, a homogenous solution of the form Eq. (4.5) should be added. Note that we use the value of the meridional velocity at $z = 100$ hPa for the upper-level boundary condition. This solution would not actually assure us that the total estimated vertical velocity at the ground would be zero [$w_{\text{part}}(z = 0) + w_{\text{homo}}(z = 0) = 0$], which is the correct linear boundary condition. For our discussion, however, it will be sufficient to use the full linear equation estimated as

$$v_{\text{linear}} = v_{\text{part}}(x, y, z) + v_{\text{baro}}(x, y, z), = \overline{U}\int_z^{100} R/\overline{U}^2\,dz + v(z = 100\,\text{hPa}) \times \exp\left[-\int_z^{100}\left(\frac{\overline{g\Theta_y}}{|f_0|\Theta_0}\right)\Big/\overline{U}(z, y)\,dz\right]. \tag{4.6}$$

The total linear response is shown for the Constant solution (black contour) in the middle graph of Fig. 10. The estimated meridional velocity $v_{\text{part}}$ for the Constant case is also shown in the middle graph of Fig. 10 (color shading). The thermal forcing tends to reduce the barotropic poleward/equatorward flow of the solutions at lower levels. We could also use the expression (4.5) to estimate the vertical structure of the remotely generated external wave of the Control solution as well, of course, using the zonal quantities corresponding to the Control case. The linear estimate of the meridional velocity for the Control run is shown on the top graph of Fig. 10. It should be noted that the Control meridional velocity tends to be more barotropic than the Constant solution. The reason seems clear: the effect of thermal forcing produces an equatorward (poleward) flow over the positive (negative) thermal forcing area, as previously discussed. When added to the out-of-phase remotely forced external wave, this gives a smaller poleward/equatorward meridional velocity at the lower levels.

It is not as straightforward to estimate the meridional velocity for the Interactive case from the linear horizontal heat balance as for the Control case. Recall that for the Interactive case, although the time-averaged thermal forcing is the same as that used in Eq. (4.4), the thermal forcing is time dependent and proportional to the asymmetric part of the total meridional velocity as given by Eq. (3.6). The horizontal advection should be modified from Eq. (4.3) as follows:

$$-\overline{U}v_z + v\overline{U}_z = -\frac{g}{|f_0|}\kappa\frac{\overline{Q(y, z)}}{\Theta_0}\frac{v}{V_0} = -\frac{\overline{R(y, z)}}{V_0}v, \tag{4.7}$$

where $\overline{R}$ is the zonally averaged thermal forcing, which is the same as that used in the Control solution. As previously defined, $V_0$ controls the intensity of the interaction of the thermal forcing in the heat equation for the solution under discussion, $V_0 = 2$. The solution for $v$, integrating Eq. (4.7) and replacing the vertical shear of the zonal mean flow by the thermal wind relation, gives the total linear response of the remote and local thermal forcing:

$$v(x, y, z) = v(z = 100\,\text{hPa}) \times \exp\left[-\int_z^{100}\left(\frac{\overline{R}}{V_0} + \frac{\overline{g\Theta_y}}{|f_0|\Theta_0}\right)\Big/\overline{U}(z, y)\,dz\right]. \tag{4.8}$$

As previously done, we assume that there is a remote signal at the upper levels ($z = 100$ hPa) that was unaffected by low-level local forcing. We could interpret that Eq. (4.8) represents the total ($v_{\text{homo}} + v_{\text{part}}$) linear estimate of the meridional velocity of the Interactive case. However, in a similar fashion as before we could estimate a linear equivalent barotropic solution without the thermal forcing:

$$v_{\text{baro}}(x, y, z) = v(z = 100\,\text{hPa}) \times \exp\left[-\int_z^{100}\left(\frac{\overline{g\Theta_y}}{|f_0|\Theta_0}\right)\Big/\overline{U}(z, y)\,dz\right]. \tag{4.9}$$

The difference between $v(x, y, z) - v_{\text{baro}}(x, y, z) = v_{\text{part}}$ from Eqs. (4.8) and (4.9) could be defined as the estimate of the linear meridional velocity due to the local thermal forcing for the Interactive case and is shown on the bottom graph of Fig. 10. The full linear meridional velocity

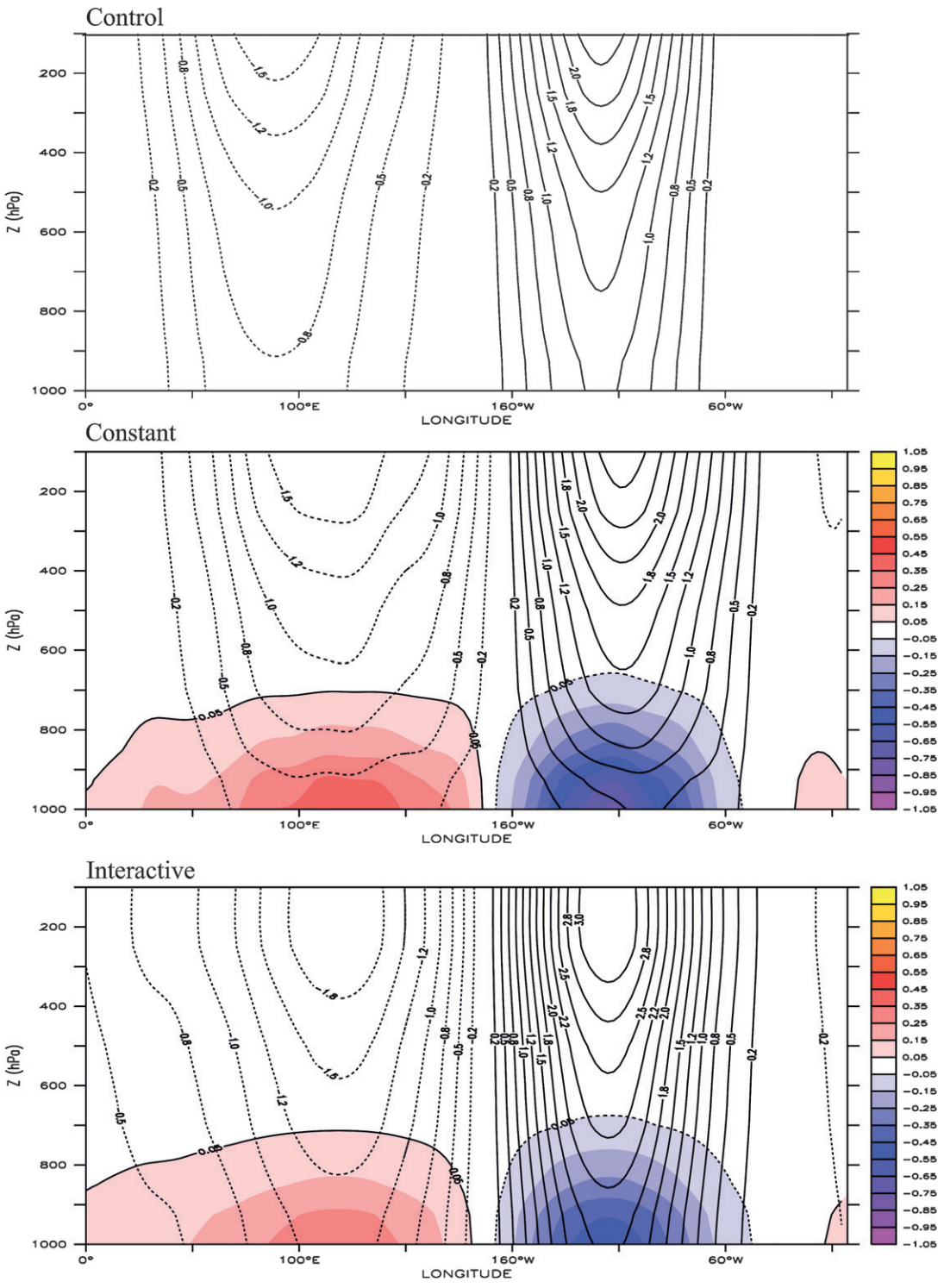


FIG. 10. The linear estimate of the meridional velocity induced by the thermal forcing in color shading (see text) and the linear meridional velocity for the external waves that are remotely and locally forced for the (a) Control, (b) Constant, and (c) Interactive cases. The local thermally forced meridional velocity has a contour of 0.1 m $s^{-1}$ and the total linear solution has a contour of 0.25 m $s^{-1}$.

is also shown [Eq. (4.8)]. There is a considerable similarity between the estimated structure of the thermal forced meridional velocity ($v_{\text{part}}$) for the Interactive and Constant solutions in the middle and bottom graphs of Fig. 10.

*d. Some transient aspects of the steady response*

To complete this discussion we should note that the linear solution explains a large part of the response. However, as we can see from Figs. 8 and 9, when the Control solution is removed from the Constant and Interactive solutions, the difference between them seems considerable. Are those differences explainable by the linear theory of the steady-state solutions? Probably not. Recall that for the steady solutions both equatorial and polar forcing are the same. As was mentioned before, the difference between these solutions is the time-dependent forcing in the Interactive run compared with the time-independent forcing in the Constant solution. Calculation of the zonal and meridional transient heat flux shows considerable differences for both simulations. The heat flux divergence from daily transients is approximately 20% of the thermal forcing magnitude and could modify the thermal forcing [as seen in Eq. (4.2)] between both solutions. While the focus of this paper is to show the possibility of the feedback in the simulations, for purposes of clarity we discussed the linear response. We feel that a thorough discussion on the role of the nonlinear effects will exceed the level of this article. We note that the time-dependent forcing seems to slightly modify the propagation of the remotely forced wave. In the linear solution cross section (Fig. 10), we see that the upper-level maximum velocity is approximately in phase between the Control and Interactive solutions, whereas the *Constant* solution shows a maximum shifted approximately 10° eastward. This result is not surprising because the parameterization depends on the total magnitude of the zonal asymmetric part of the meridional velocity. The thermal forcing depends on the so-called $v_{\text{part}} + v_{\text{baro}}$ and locks the position of the meridional velocity in the *Interactive* solution [Eq. (4.8)]. In contrast, in the Constant solution the meridional velocity response to the remote forcing is not constrained to be in phase with the local thermal forcing response as it is for the Interactive case. From another point of view, a simple way to illustrate the propagation difference between these solutions is by making use of the time-averaged **E** vectors (Hoskins et al. 1985; Kiladis 1998, among others). The **E** vector is a statistical measure of the mean dispersion characteristics of Rossby wave activity and is constructed by calculating time-mean covariance between the perturbation zonal and meridional component of the wind. Together the two components approximate the preferred direction of the group velocity of the waves:

$$\mathbf{E} = (\overline{v^2} - \overline{u'^2},\ -\overline{u'v'}). \tag{4.10}$$

The results seems to suggest that the difference between the Constant and Interactive solutions arises not so much from the local circulation the thermal forcing produces, but rather from modifying the wave propagation from the remote source. Note that the barotropic component [Eqs. (4.6) and (4.9)] only produces the vertical structure of the linear response, whereas the phase difference between the two cases is contained in the boundary condition $v(z = 100\ \text{hPa})$ that has been used to calculate the linear estimate shown in Fig. 10. For that reason it will be instructive to show the upper levels of **E** vectors for both cases as well as for the difference with the Control case. Figure 11 shows (top) the 300-hPa **E** vectors and the geopotential heights for both solutions and (bottom) their differences with the Control solution. The **E** vector shown contains only the time mean of the transient eddies. Note the large **E**-vector response over the storm track region at the latitudinal band between 20° and 40°S, for both solutions. The tropical remote forcing tends to leak through the storm-track band with the **E** vector showing an east-poleward direction. The notable difference between the responses of the Constant − Control and the Interactive − Control solutions seems to be due to the fact that the transient eddies on the time-dependent forcing in Interactive − Control disorganize the propagation of the Rossby waves. This contrasts with the Constant − Control solution that displays a more coherent **E** vector pointing to the southeast direction.

Finally, let us comment about the variability of the feedback with $V_0$. We mentioned earlier that we performed different runs varying the amplitude of the interactive coefficient $V_0$. The qualitative results of the different simulations are very similar. However, as expected, the amplitude of the response increases as the interaction coefficient increases: $1/V_0 = 0.1, 0.2, 0.33, 0.5$ ($V_0 = 10, 5, 3, 2$). Figure 12 shows the dependence of the maximum geopotential height at 300 hPa with the interactive value $V_0$. For $V_0$ larger than 3 (all the previous figures show the solutions for $V_0 = 2$), the solution seems to grow linearly with the inverse of $V_0$ and tends to level off for smaller values. The main reason is that the nonlinear eddy becomes very strong and reduces the thermal forcing efficiency, as hinted from Eq. (4.2).

## 5. Summary and discussion

We illustrate how a quasi-stationary wave can be intensified by a thermal source, usuallydue to latent heating by convection or other eddy-induced diabatic heating.

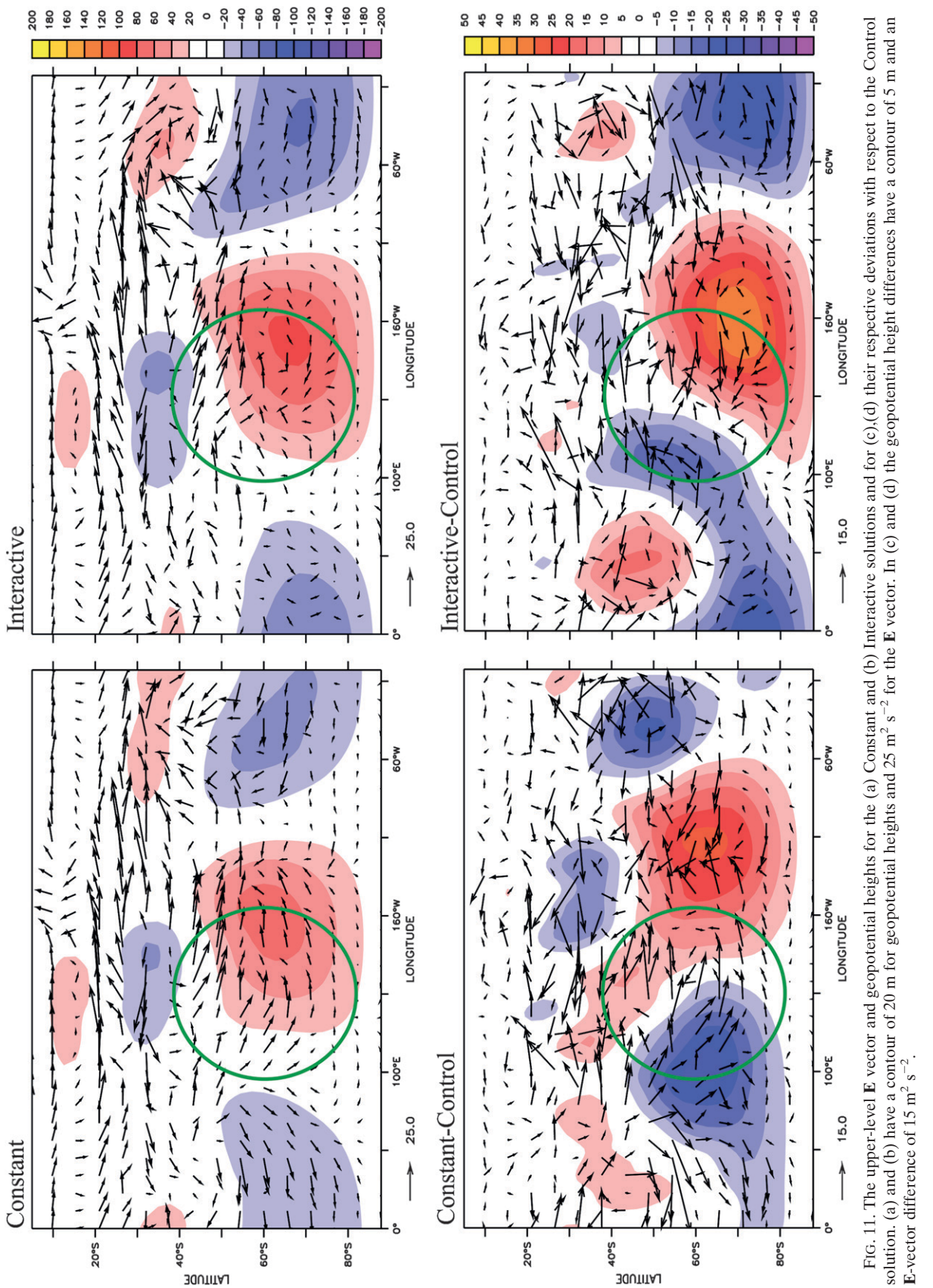


FIG. 11. The upper-level **E** vector and geopotential heights for the (a) Constant and (b) Interactive solutions and for (c),(d) their respective deviations with respect to the Control solution. (a) and (b) have a contour of 20 m for geopotential heights and 25 $m^2 s^{-2}$ for the **E** vector. In (c) and (d) the geopotential height differences have a contour of 5 m and an **E**-vector difference of 15 $m^2 s^{-2}$.

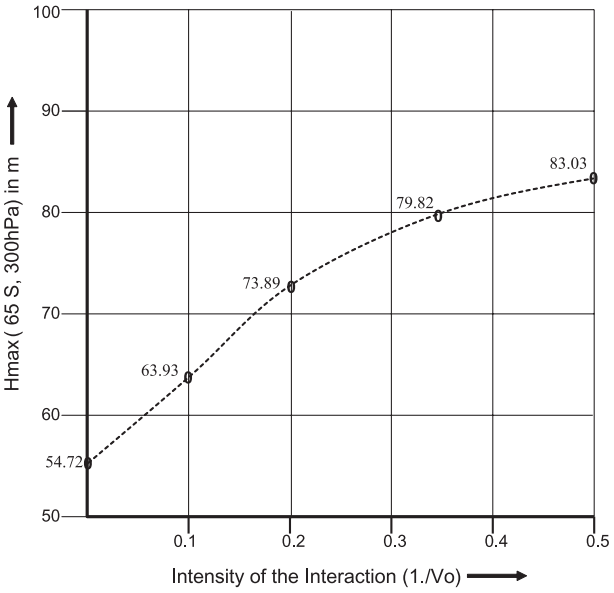


FIG. 12. Geopotential height maximum for the stationary response as a function of the interactive coefficient $1/V_0$. The height maximum was measured over the latitude of maximum thermal forcing (65°S).

Moreover, under some conditions the circulation of the equivalent barotropic wave could organize a convective region and enhance the thermal forcing by supplying moisture to the area of convection. This process of mutual interaction could explain the persistent large amplitude of external Rossby waves, despite the diffusive effects that high frequency eddies can exert on these waves. For this study, we chose the quasi-stationary patterns that are observed on the southeastern Pacific Ocean and the periphery of Antarctica.

As an example, we have discussed a recurrent pattern over the southeastern Pacific Ocean in the proximity of the Bellingshausen and Amundsen Seas. A high anomaly is detected in that region and has been associated not only with the PSA pattern linked to the warm phase of ENSO but with other natural variability modes that excite similar patterns as well. In particular, the regression of the low-level horizontal wind pattern, potential temperature, and relative humidity fields against El Niño 3.4 time series displays a consistent picture. The regression pattern indicates that the area of convective activity seems to appear at the southwestern side of the high pattern where moist warm air is blown over colder SSTs, sea ice, and the Antarctic coast, producing the observed convection.

A different, but also consistent, picture results from the analysis of two AGCM simulations: one with sea ice and one without. The lack of sea ice close to the Ross Sea produces a high anomaly similar to that of the PSA pattern. The spatial pattern of the diabatic heating that was obtained from the convective activity is similar to that of precipitation with respect to the geopotential high. In both cases, the structure of the external Rossby waves has definitively a barotropic equivalent structure, without much phase change in the vertical. We suggest that these waves could have been enhanced by thermal forcing of the convective regions that they themselves organized.

A series of experiments has been carried out with a dynamic core of a global spectral model so as to evaluate the possibility of a positive feedback between the external wave and a thermal forcing. The main thrust of the paper is based on the results with an idealized feedback to the thermal forcing, which depends on the low-level meridional velocity strengthening or weakening the thermal forcing. The feedback of the thermal forcing has some similarity to the well-known formulation of wave-CISK. However, where in that case the convection is excited by surface convergence, as it is common in the tropics, in this case the convection is more correlated with the horizontal advection of heat and moisture.

Three experiments—all forced with a tropical heat source able to produce an external Rossby wave propagating to the high latitudes of both hemispheres, similar to a warm ENSO event—were done for a quantitative estimation of the feedback of thermal forcing and the external wave: (i) the Control experiment with a zonal heat source in subpolar latitudes has a similar climatology to the sensitivity experiments, (ii) the Interactive simulation with a time-dependent forcing, and (iii) the Constant run in which the heat source used was derived from the long time-averaged solution of the Interactive case.

Both sensitivity simulations tend to show an increase of the response amplitude in the upper levels when compared with the Control run, with the interactive forcing solution displaying the largest amplitude. It seems that the quasi-linear analysis could explain the qualitative features of the waves. Although we did not expand in the nonlinear aspects of remotely generated external Rossby waves, it seems that the time-dependent evolution could modify the remote response, as shown in the patterns of the Interactive and Constant runs. It seems that the transient heat flux divergence reduced the thermal forcing and the actual propagation path of the remotely generated external waves is affected by the transient eddies. These issues are very important when external Rossby waves are in the proximity of storm tracks. Work on these lines will be published elsewhere.

The simulations also show that considerable amplification can be obtained by increasing the feedback forcing.

Although we chose a particular region for the purpose of explaining this process, it is clear that these phenomena

could occur in any region where such circulation is excited. More studies are required to simulate other conditions over the globe that could be favorable for these types of interactions. Also, the preferred time scale for such interaction requires further study.

*Acknowledgments.* We thank Isaac Held for providing us with a version of the core GFDL spectral global model and discussions that helped clarify and focus this research. Bruce Wyman provided us with the AM2 GCM solutions for the sea ice and No–sea ice simulations and Peter Phillipps implemented changes to the spectral model. I would also like to extend my appreciation to Isaac Held and Kar Mac Chang for reviewing the manuscript. In addition, we also would like to thank Sara Mikaloff-Fletcher for editing and comments that help clarify the manuscript. The thorough review of three anonymous reviewers that helped enormously in clarifying the present revision is greatly appreciated.

One of the authors, Isidoro Orlanski, was supported under Awards NA17RJ2612 and NA08OAR4320752 from the National Oceanic and Atmospheric Administration, U.S. Department of Commerce. The statements, findings, conclusions, and recommendations are those of the author(s) and do not necessarily reflect the views of the National Oceanic and Atmospheric Administration or the U.S. Department of Commerce.

Silvina Solman's research has been supported by ANPCyT Grant PICT2005 32194 and UBACyT Grant X160.

## REFERENCES

Ambrizzi, T., B. Hoskins, and H. H. Hsu, 1995: Rossby wave propagation and teleconnection patterns in the austral winter. *J. Atmos. Sci.,* **52,** 3661–3672.

Anderson, J. L., and Coauthors, 2004: The new GFDL global atmosphere and land model AM2-LM2: Evaluation with prescribed SST simulations. *J. Climate,* **17,** 4641–4673.

Blackmon, M. L., R. A. Madden, J. M. Wallace, and D. S. Gutzer, 1979: Geographical variations in the vertical structure of geopotential height fluctuations. *J. Atmos. Sci.,* **36,** 2450–2466.

Bolin, B., 1950: On the influence of the earth's orography on the general character of the westerlies. *Tellus,* **2,** 184–195.

Charney, J. G., and A. Eliassen, 1949: A numerical method for predicting the perturbations of the middle-latitude westerlies. *Tellus,* **1,** 38–54.

——, and ——, 1964: On the growth of the hurricane depression. *J. Atmos. Sci.,* **21,** 69–75.

Deser, C., R. A. Tomas, and S. Peng, 2007: The transient atmospheric circulation response to North Atlantic SST and sea ice anomalies. *J. Climate,* **20,** 4751–4767.

Dole, R. M., 1983: Persistent anomalies of extratropical Northern Hemisphere wintertime circulation. *Large-Scale Dynamical Processes in the Atmosphere,* B. Hoskins and R. Pearce, Eds., Academic Press, 95–109.

Egger, J., 1976: The linear response of a hemispheric two-level primitive equation model to forcing by topography. *Mon. Wea. Rev.,* **104,** 351–364.

Gao, X. H., and J. L. Stanford, 1988: Possible feedback path for low-frequency atmospheric oscillations. *J. Atmos. Sci.,* **45,** 1425–1432.

Grose, W. L., and B. J. Hoskins, 1979: On the influence of orography on the large-scale atmospheric flow. *J. Atmos. Sci.,* **36,** 223–234.

Held, I. M., 1983: Theory of stationary eddies. *Large-Scale Dynamical Processes in the Atmosphere,* B. Hoskins and R. Pearce, Eds., Academic Press, 127–168.

——, and M. Ting, 1990: Orographic versus thermal forcing of stationary waves: The importance of the mean low-level wind. *J. Atmos. Sci.,* **47,** 495–500.

——, and M. Suarez, 1994: A proposal for the intercomparison of the dynamical cores of atmospheric general circulation models. *Bull. Amer. Meteor. Soc.,* **75,** 1825–1830.

——, R. Pierrehumbert, and R. L. Panetta, 1986: Dissipative destabilization of external Rossby waves. *J. Atmos. Sci.,* **43,** 388–396.

Hendon, H. H., and D. L. Hartmann, 1982: Stationary waves on a sphere: Sensitivity to thermal feedback. *J. Atmos. Sci.,* **39,** 1906–1920.

Holopainen, E. O., L. Rontu, and N. C. Lau, 1982: The effect of large-scale transient eddies on the time-mean flow in the atmosphere. *J. Atmos. Sci.,* **39,** 1972–1984.

Honda, M., K. Yamazaki, H. Nakamura, and K. Takeuchi, 1999: Dynamic and thermodynamic characteristics of atmospheric response to anomalous sea-ice extent in the sea of Okhotsk. *J. Climate,* **12,** 3347–3358.

Horel, J. D., and J. M. Wallace, 1981: Planetary-scale atmospheric phenomena associated with the Southern Oscillation. *Mon. Wea. Rev.,* **109,** 813–829.

Hoskins, B. J., and D. J. Karoly, 1981: The steady linear response of a spherical atmosphere to thermal and orographic forcing. *J. Atmos. Sci.,* **38,** 1179–1196.

——, I. N. James, and G. H. White, 1985: The shape, propagation and mean-flow interaction of large-scale weather systems. *J. Atmos. Sci.,* **40,** 1595–1612.

Kasahara, A., 1966: The dynamical influence of orography on the large-scale motion of the atmosphere. *J. Atmos. Sci.,* **23,** 259–271.

——, T. Sasamori, and W. Washington, 1973: Simulation experiments with a 12-layer stratospheric global circulation model. I. Dynamical effect of the earth's orography and thermal influence of continentality. *J. Atmos. Sci.,* **30,** 1229–1251.

Kiladis, G. N., 1998: Observations of Rossby waves linked to convection over the eastern tropical Pacific. *J. Atmos. Sci.,* **55,** 321–339.

Kushner, Y., W. A. Robinson, I. Bladé, N. M. Hall, S. Peng, and R. Sutton, 2002: Atmospheric GCM response to extratropical SST anomalies: Synthesis and evaluation. *J. Climate,* **15,** 2233–2256.

Lau, N. C., 1979: The observed structure of tropospheric stationary waves and the local balances of vorticity and heat. *J. Atmos. Sci.,* **36,** 996–1016.

Lindzen, R. S., 1974: Wave-CISK in the tropics. *J. Atmos. Sci.,* **31,** 156–179.

Manabe, S., and T. B. Terpstra, 1974: The effects of mountains on the general circulation of the atmosphere as identified by numerical experiments. *J. Atmos. Sci.,* **31,** 3–42.

Mo, K. C., and G. H. White, 1985: Teleconnections in the Southern Hemisphere. *Mon. Wea. Rev.,* **113,** 22–37.

——, and M. Ghil, 1987: Statistics and dynamics of persistent anomalies. *J. Atmos. Sci.,* **44,** 877–901.

——, and R. W. Higgins, 1998: The Pacific–South American modes and tropical convection during the Southern Hemisphere winter. *Mon. Wea. Rev.,* **126,** 1581–1596.

——, and J. N. Paegle, 2001: The Pacific–South American modes and their downstream effects. *Int. J. Climatol.,* **21,** 1211–1229.

Namias, J., 1973: Response of the equatorial countercurrent to the subtropical atmosphere. *Science,* **181,** 1244–1245.

Plumb, R. A., 1985: On the three-dimensional propagation of stationary waves. *J. Atmos. Sci.,* **42,** 217–229.

Randel, W. J., and J. L. Stanford, 1983: Structure of medium-scale atmospheric waves in the Southern Hemisphere summer. *J. Atmos. Sci.,* **40,** 2312–2318.

Silvestri, G. E., and C. S. Vera, 2003: Antarctic Oscillation signal on precipitation anomalies over southeastern South America. *Geophys. Res. Lett.,* **30,** 2115, doi:10.1029/2003GL018277.

Simmonds, I., and T. H. Jacka, 1995: Relationship between the interannual variability of Antarctic sea ice and the Southern Oscillation. *J. Climate,* **8,** 637–647.

Smagorinsky, J., 1953: The dynamical influence of large-scale heat sources and sinks on the quasi-stationary mean motions of the atmosphere. *Quart. J. Roy. Meteor. Soc.,* **79,** 342–366.

Trenberth, K. E., 1980: Planetary waves at 500 mb in the Southern Hemisphere. *Mon. Wea. Rev.,* **108,** 1378–1389.

Venegas, S. A., and M. R. Drinkwater, 2001: Sea ice, atmosphere and upper ocean variability in the Weddell Sea, Antarctica. *J. Geophys. Res.,* **106,** 16 747–16 765.

Wallace, J. M., and D. S. Gutzler, 1981: Teleconnections in the geopotential heights field during the Northern Hemisphere winter. *Mon. Wea. Rev.,* **109,** 784–812.

——, and M. L. Blackmon, 1983: Observations of low-frequency atmospheric variability. *Large-Scale Dynamical Processes in the Atmosphere,* B. Hoskins and R. Pearce, Eds., Academic Press, 55–94.

Watanabe, E., and H. Hasumi, 2005: Arctic sea ice response to wind stress variations. *J. Geophys. Res.,* **110,** C11007, doi:10.1029/2004JC002678.

White, W. B., and R. G. Peterson, 1996: An Antarctic circumpolar wave in surface pressure, wind, temperature and sea-ice extent. *Nature,* **380,** 699–702.

Youngblut, C., and T. Sasamori, 1980: The nonlinear effects of transient and stationary eddies on the winter mean circulation. Part I: Diagnostic analysis. *J. Atmos. Sci.,* **37,** 1944–1957.

Yuan, X., 2004: ENSO-related impacts on Antarctic sea ice: A synthesis of phenomenon and mechanisms. *Antarct. Sci.,* **16,** 415–425.